Mechanism of the atmospheric chemical transformation of acetylacetone and its implications in night-time second organic aerosol formation

Yuemeng Ji [a], Dandan Qin [a], Jun Zheng [b], Qiuju Shi [a], Jiaxin Wang [a], Qinhao Lin [a], Jiangyao Chen [a], Yanpeng Gao [a], Guiying Li [a], Taicheng An [a,*]

[a] Guangdong Key Laboratory of Environmental Catalysis and Health Risk Control, School of Environmental Science and Engineering, Institute of Environmental Health and Pollution Control, Guangdong University of Technology, Guangzhou 510006, China
[b] Collaborative Innovation Center of Atmospheric Environment and Equipment Technology, Nanjing University of Information Science & Technology, Nanjing 210044, China

HIGHLIGHTS

- The ozonolysis of AcAc is more significant than the AcAc+NO$_3$ reaction.
- O$_3$-addition to AcAc, as the predominant pathway, produces SOA precursors.
- The nighttime chemistry of AcAc is of importance to SOA formation.
- Oxidation of AcAc successively contributes to SOA formation in polluted areas.

GRAPHICAL ABSTRACT
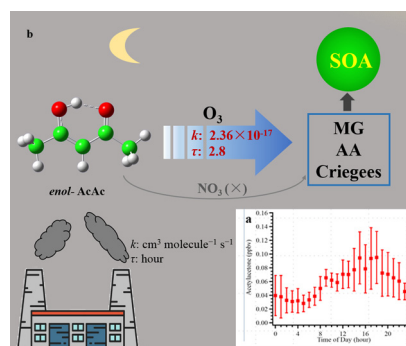
ARTICLE INFO

ABSTRACT

Recently, a high concentration of acetylacetone (AcAc) has been measured in China, and its day-time chemistry with •OH reaction has been evaluated. The phenomenon has profound implications in air pollution, human health and climate change. To systematically understand the atmospheric chemistry of AcAc and its role in the atmosphere, the night-time chemistry of AcAc with O$_3$ and NO$_3$ radical were investigated in this work in detail using density functional theory. The results show that for O$_3$- and NO$_3$-initiated atmospheric oxidation reactions of AcAc, the barrier energies of O$_3$/NO$_3$-addition are found to be much lower than those of H-abstraction, suggesting that O$_3$/NO$_3$-addition to AcAc is a major contributing pathway in the atmospheric chemical transformation reactions. The total degradation rate constants were calculated to be 2.36×10^{-17} and 1.92×10^{-17} cm^3 molecule^{-1} s^{-1} for the O$_3$- and NO$_3$-initiated oxidation of AcAc at 298 K, respectively. The half-life of AcAc +O$_3$ in some polluted areas (such as, Pearl River Delta and Yangtze River Delta) is close to 3 h under typical tropospheric conditions. Due to its short half-life, the ozonolysis of AcAc plays a more significant role in the night-time hours, leading to fast transformations to form primary ozonides (POZs). A prompt, thermal decomposition of POZs occurred to yield methylglyoxal, acetic acid and Criegee intermediates, which mainly contributed to the formation of secondary organic aerosol (SOA). Subsequently, using the high-resolution time-of-flight chemical ionization mass spectrometer (HR-ToF-CIMS), a non-negligible concentration of AcAc was measured in the field observation during the night-time in Nanjing, China. The obtained results reveal that the atmospheric oxidation of AcAc can successively contribute to the formation of SOA under polluted environments regardless of the

* Corresponding author.
E-mail address: antc99@gdut.edu.cn (T. An).

time (day-time or night-time). This is due to its high reactivity to tropospheric oxidant species (such as, O_3 and NO_3 radicals at night-time).

1. Introduction

In recent years, field measurements have revealed a high concentration of acetylacetone (AcAc) in two mega-cities (Beijing and Nanjing) in China (Ji et al., 2018). The measured concentration of AcAc varies from several hundred parts per trillions to several parts per billions, and such high concentrations clearly indicate a critical role of AcAc in the atmospheric chemistry (Ji et al., 2018). Furthermore, AcAc is a common *diketone* (also known as 2,4-pentanedione), and is used in industrial applications due to its high reactivity. Therefore, AcAc is an important substrate, and has been widely used in various industrial applications. For example, it is used as a bidentate ligand, a chelating agent, or a reagent for the preparation of chelating compounds for a wide range of transition metals (Tsujimoto et al., 2001; Hollmann et al., 2008; Raykar and Singh, 2010; Ho et al., 2015; Warneke et al., 2015).

In a previous theoretical work, it was reported that a high yield (more than 66%) of SOA precursors was obtained from •OH-initiated oxidation intermediates of AcAc during day-time, and included methylglyoxal (MG), acetic acid (AA) and peroxyacetyl nitrate (PAN) (Ji et al., 2018). These products were also identified and confirmed by an earlier experimental study using a relative kinetic method (Zhou et al., 2008). Among these products, the oligomerization of small α-dicarbonyls represents a major source of SOA on urban, regional, and global scales (Tan et al., 2009; Zarzana et al., 2012; Marrero-Ortiz et al., 2019). Additionally, organic acids and MG also play important roles in the formation and growth of novel nanoparticles (Zhang et al., 2004b; Tan et al., 2012; Zhang et al., 2015; Ji et al., 2017; Sareen et al., 2017). All the evidence indicated that the •OH-initiated reaction of AcAc contributes to the formation of tropospheric SOA and O_3 (Shrivastava et al., 2017). Particularly, SOA formed in the atmosphere by the oxidation of organic gases represents a major fraction of global submicron-sized atmospheric organic aerosols. However, the mechanism of atmospheric oxidation of ketone is still not completely understood by a variety of oxidant species, including resulted O_3 and NO_3, as well as halogen radicals (Aschmann et al., 1996; Finlayson-Pitts and Pitts, 1997; Mellouki et al., 2015). In particular, O_3 and NO_3 radicals are critical reactive oxidant species during night-time hours to initiate the atmospheric chemistry of volatile organic compounds (VOCs) (Mellouki et al., 2003). Hence, to systematically assess the role of AcAc in the formation of SOA, the mechanism of the atmospheric chemical transformation of AcAc involving ozone and nitrate radicals needs to be understood. Although a few studies have already focused on the atmospheric chemistry of AcAc involving ozone and nitrate radicals, the results on the mechanism and the kinetics are still controversial. For example, the rate constant of AcAc with O_3 has been estimated to be $(1.03 \pm 0.31) \times 10^{-18}$ cm^3 molecule^{-1} s^{-1} at 298 K with the chamber experiments (Zhou et al., 2008), which is twice of the rate constant $(5.23 \pm 0.18) \times 10^{-19}$ cm^3 molecule^{-1} s^{-1} determined experimentally (Holloway et al., 2006). Zhou et al. (2008) reported a long life-time (16.1 days) of AcAc using average tropospheric O_3 concentrations ($[O_3]$) (Logan, 1985). However, in some polluted countries (such as, China), the average tropospheric $[O_3]$ is ten times higher than that of the global data (Wang et al., 2017; Liu et al., 2018). Additionally, ozonolysis of VOCs has been regarded as a large source of low-volatility SOAs (Ehn et al., 2014; Rissanen et al., 2014). However, to the best of our knowledge, no systematic theoretical study is available to understand the reaction mechanisms of atmospheric AcAc with O_3/NO_3.

In the current study, the night-time chemistry of AcAc with O_3 and NO_3 radicals was investigated in detail and the contributions of these radicals to the formation of night-time SOAs was evaluated. The detailed reaction mechanisms were successfully established using quantum chemical approach, and the kinetic data including the rate constant, the product distribution and the half-life of AcAc within the atmosphere were determined using canonical variational transition state theory (CVT) with the small curvature tunneling (SCT) (Fernandez-Ramos et al., 2007). The fate of atmospheric AcAc was systematically assessed, and the implications of the atmospheric chemistry of AcAc during the formation of SOA were also discussed.

2. Methodology

All the calculations were performed by employing the Gaussian 09 software package (Frisch et al., 2009). The geometric optimizations of all stationary points (SPs), such as reactants, products and transition states (TSs) were performed at the M06-2X level with a standard 6-311G(d,p) basis set (M06-2X/6-311G(d,p)). In order to validate the convergence of the predicted geometries, the geometries were also optimized at the MP2/ and B3LYP/6-311G(d,p) levels, which represent the classic Ab Initio and density functional theory, respectively. The frequency calculations were performed to identify either TS (with one and only one imaginary frequency) or a real minimum (with no imaginary frequency) and to make zero-point energy corrections (ZPE). All the optimized geometries represent the minimum on the potential energy surface (PES) and were confirmed by the evaluation of the vibrational frequencies (Tables S1 and S2). The minimum-energy path (MEP) was constructed to verify that, each TS connected the reactants ($AcAc+O_3/AcAc+NO_3$) with the corresponding products by intrinsic reaction coordinate (IRC) theory. The PES was refined at the M06-2X/6-311++G(3df,3pd) level to obtain more accurate energetics.

The duel-level direct dynamics were carried out along the reaction path using the interpolated single point energy (SPE) method (Chuang et al., 1999; Ji et al., 2012), in which extra single-point calculations near the TS along the MEP were performed to obtain the kinetic information. By means of the Polyrate program (Zheng et al., 2010), the rate constants were obtained according to the CVT with SCT (Ji et al., 2013; Wang et al., 2015). For a pathway that has a defined barrier, the rate constant was obtained using Eqs. (1) and (2) (Ji et al., 2018).

$$k^{GT}(T,s) = \sigma \frac{k_B T}{h} \frac{Q^{TS}(T)}{Q^R(T)} \exp\left[-\frac{v^*(MEP)}{k_B}T\right] \tag{1}$$

$$k^{CVT} = \min_s k^{GT}(T,s) \tag{2}$$

where s is the location of the generalized TS on IRC, σ is the symmetry factor related to the degeneracy of reaction path, and k_B and h are the Boltzmann and Planck's constants, respectively. Additionally, $Q^R(T)$ denotes the total partition functions of the reactants, and $Q^{TS}(T)$ denotes the classical generalized transition state partition function, which is expressed in per unit volume. Furthermore, $v^*(MEP)$ is equal to the zero of energy for the generalized transition state partition function is taken as the minimum of the local vibrational modes orthogonal to the reaction path at s. In order to account for the tunneling effect, the CVT rate constant was multiplied by a multiplicative transmission coefficient computed with the so-called Winger correction. The partition function was calculated using the hindered rotor approximation of Truhlar and Chuang. The effective reduced mass is obtained by a sixth-order Lagrangian interpolation for SCT calculations.

The half-life was determined using the correlation: $\tau = \frac{1}{k_{total}[O_3/NO_3]}$ (Hoigne and Bader, 1978), where $[O_3/NO_3]$ and k_{total} are the

concentration of O_3 or NO_3 and the corresponding total CVT/SCT rate constant, respectively. The parametrization method (Gao et al., 2019) was used to estimate the production of SOA according to the correlation: $SOA_{par} = P_{pre} \times Y_i$, where P_{pre} corresponds to the amount of precursors from AcAc reaction with O_3, and Y_i is the SOA yield (Zhang et al., 2016) from the consumed P_{pre}. The P_{pre} can be deduced using the correlation: $P_{pre} = k \times t \times [VOC] \times [Oxidant]$ (Yuan et al., 2013), where [VOC] and [Oxidant] represent the concentrations of AcAc and the oxidant (O_3 or NO_3 radical), respectively, k is the rate constant of AcAc reaction with O_3 or NO_3, and t is the night-time hours.

3. Results and discussion

3.1. Initial reaction of AcAc with O_3 and NO_3 radicals

In order to provide a systematic mechanism, the reactions of *enol*-AcAc and *keto*-AcAc with O_3 and NO_3 radicals were considered because both the *enolic* and *ketonic* isomers of AcAc (*enol*-AcAc and *keto*-AcAc) exist in the system (Nagashima et al., 2001; Broadbent et al., 2007; Trivella et al., 2007). Two distinct reaction pathways were observed depending on how the radicals attacked the active site of AcAc (as shown in Figs. 1 and S1). These reaction pathways corresponded to O_3- and

NO_3-addition to the carbonyl position of AcAc (e/k-R_{add}) and H-abstraction from the two methyl groups of AcAc (e/k-R_{abs}). Figs. S2 and S3 present the optimized geometries of all the SPs in the AcAc $+O_3$ and AcAc$+NO_3$ reaction systems, along with the available experimental data (Ishiwata et al., 1985) and the results obtained at the calculation levels of MP2/ and B3LYP/6-311G(d,p). Based upon the results, it was concluded that the calculated results agreed well with the experimental data. The largest discrepancies among the three methods were within 0.9° in the bond angles and 0.07 Å in the bond lengths. This suggests that the reliable geometrical optimization is conducted by the M06-2X method for the current reaction systems. Table S1 lists the vibrational frequencies, absolute energies, Cartesian coordinates, and the ZPEs of the relevant species.

The PESs of all possible pathways for the reactions of AcAc with O_3 and NO_3 radicals are presented in Figs. 1 and S1, respectively. The addition of O_3 occurs in a concerted fashion at the two double bonds of AcAc, i.e., the >C=C< for *enol*-AcAc or the >C=O< for *keto*-AcAc, thus leading to the formation of two distinct structural primary ozonides (POZ1 and POZ2, Fig. S2). For *enol*-AcAc, the reaction proceeds through two cyclization pathways, namely the e-R_{add}1 and e-R_{add}2, depending on the O_3 addition to the different orientations of AcAc, to form the adducts of POZ11 and POZ12, respectively. As shown in Fig. 1, the energy barriers (ΔE)
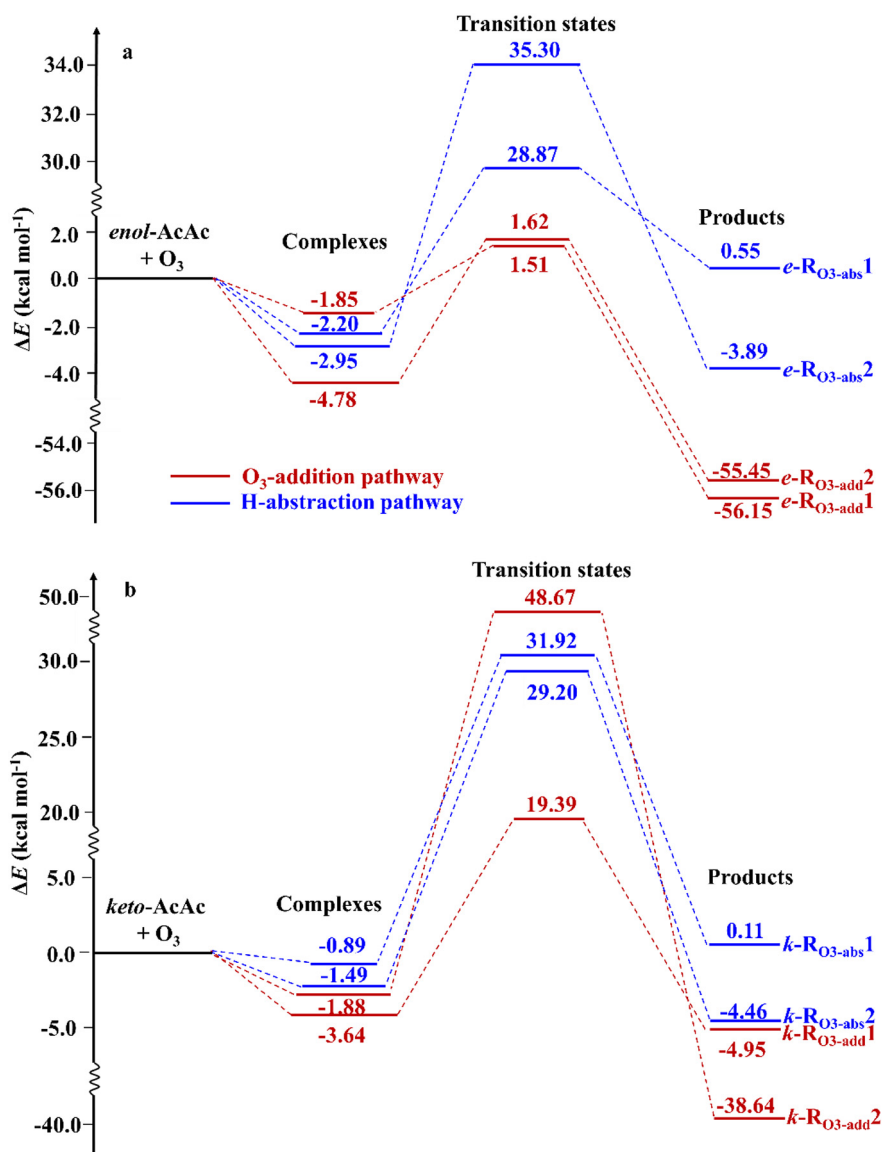

Fig. 1. PES of the reactions of (a) *enol*-AcAc and (b) *keto*-AcAc with O_3 (unit: kcal mol^{-1}).

were found to be 1.51 and 1.62 kcal mol^{-1} for e-R$_{add}$1 and e-R$_{add}$2, respectively, which correspond to large exothermicity with 56.15 and 55.45 kcal mol^{-1}. In order to assess the reliability of M06-2X results, the energetic parameters were evaluated at the CCSD(T) method, which is costly and high-level single-point energy calculation. At the CCSD(T)/6−311 + G(2df,2p)//M06-2X/6-311G(d,p) level, the energy barrier was found to be 1.10 kcal mol^{-1}, which agrees well with the value obtained at the M06-2X//M06-2X level. Furthermore, the reaction energy of −44.28 kcal mol^{-1} was slightly higher than the current data. In addition, the M06-2X method has already been verified to be suitable for the AcAc+OH reaction system (Ji et al., 2018). All these results suggest that the M06-2X method is suitable for predicting the mechanisms and kinetic calculations of AcAc reaction system. Therefore, to achieve a balance between the computational accuracy and the cost, and to systematically understand the atmospheric chemistry of AcAc, the M06-2X method was chosen to perform the calculations.

Two pre-reactive complexes were identified prior to the corresponding TS. The structures were similar to those of the reactants, except that the forming bonds were elongated to be 2.77 and 2.87 Å for the e-RC$_{O3-add}$1 and e-RC$_{O3-add}$2 (Fig. S2), respectively. The reaction energies of e-RC$_{O3-add}$1 and e-RC$_{O3-add}$2 were lower than those of the reactants by 1.85 and 4.78 kcal mol^{-1}, respectively. The H-abstraction pathways possessed higher barriers (around 28.87 kcal mol^{-1}) than those of the O$_3$-addition pathways. The difference of the energy barriers between the H-abstraction and O$_3$-addition (more than 27 kcal mol^{-1}) suggests that the H-abstraction pathway is dynamically negligible. For $keto$-AcAc+O$_3$ reaction system, both the H-abstraction and O$_3$-addition pathways possessed higher energy barriers (around 19.39–-48.67 kcal mol^{-1}) as compared to those in the $enol$-AcAc+O$_3$ reaction system (1.51 and 1.62 kcal mol^{-1}). For example, the ΔE of the dominant pathway k-R$_{O3-add}$2 was 19.39 kcal mol^{-1} (Fig. 1), which is still larger than those of the pathways by 17.77 kcal mol^{-1} for O$_3$-addition to $enol$-AcAc.

As shown in Fig. S1, the pathway of NO$_3$ addition to $enol$-AcAc proceeded a negative ΔE with the value of −4.74 kcal mol^{-1}. However, prior to the corresponding TS, there was a pre-reactive complex (e-RC$_{NO3-add}$1), which represented a deep well with the ΔE value of −11.82 kcal mol^{-1}. In this case, the energy barrier was considered as the energy difference between the complex and the corresponding TS (ΔE = 7.08 kcal mol^{-1}). This suggests that the progress of the addition of NO$_3$ to $enol$-AcAc was hindered by this pre-reactive. Therefore, this pathway was expected not to be favorable dynamically, though the pathway had a negative energy barrier. The ΔE of the two H-abstraction pathways (e-R$_{NO3-abs}$1 and e-R$_{NO3-abs}$2) were determined to be 3.54 and 3.00 kcal mol^{-1}, respectively, which were at least 7.74 kcal mol^{-1} higher than those of the NO$_3$-addtion pathway. This suggests that NO$_3$ addition to $enol$-AcAc is more favorable than the corresponding H-abstraction pathways. However, NO$_3$ addition to $keto$-AcAc possessed a higher barrier than those of the H-abstraction pathways. For example, the ΔE of the NO$_3$-addtion pathway (8.35 kcal mol^{-1}) was higher than that of the k-R$_{NO3-abs}$2 by 4.37 kcal mol^{-1}.

As discussed above, compared to $keto$-AcAc, $enol$-AcAc prefers more to be attacked by O$_3$ and NO$_3$ radicals. For example, the dominant pathway e-R$_{O3-add}$1 or e-R$_{NO3-add}$1 in the $enol$-AcAc reaction system possessed a lower barrier (around 1.51 or − 4.74 kcal mol^{-1}) than that of the corresponding pathway in the $keto$-AcAc reaction system (around 19.39 or 8.35 kcal mol^{-1}). This behavior is explained by the conjugative effect of $enol$-AcAc (Zhou et al., 2008), indicating that $enol$-AcAc prefers being attacked by O$_3$ and NO$_3$ radicals. Previous studies (Antonov et al., 2019) have revealed the exclusive existence of AcAc as the $enol$-isomer ($ca.$ 90%), whereas the O$_3$− and NO$_3$-initiated oxidations of $enol$-AcAc are of significant importance in the atmosphere. In addition, because the conjugated π-electron character of $enol$-AcAc activates the reactivity of C atoms, the O$_3$/NO$_3$-addition to $enol$-AcAc is an exclusive pathway compared with the H-abstraction of $enol$-AcAc.

Therefore, the rate constants of O$_3$/NO$_3$ addition to $enol$-AcAc (e-R$_{O3-add}$1/2 and e-R$_{NO3-add}$1) were calculated and summarized in Fig. 2 and Table S3. The rate constants of the e-R$_{O3-add}$1 and e-R$_{O3-add}$2 were determined to be 1.43 × 10^{-17} and 9.36 × 10^{-18} cm^3 molecule^{-1} s^{-1} at 298 K, respectively. The contribution of the e-R$_{O3-add}$2 to the total rate constant was about 40% within the whole temperature range of 216–298 K (Table S4). The calculated total rate constant of the AcAc +O$_3$ reaction (k_{total}; the sum of calculated rate constants for the e-R$_{O3-add}$1 and e-R$_{O3-add}$2 pathways) is depicted in Fig. 2b. The $k_{O3-total}$ was determined to be 2.36 × 10^{-17} cm^3 molecule^{-1} s^{-1} at 298 K, which is somewhat larger than the corresponding experimental values of (1.03 ± 0.31) × 10^{-18} and (5.23 ± 0.18) × 10^{-19} cm^3 molecule^{-1} s^{-1} (Holloway et al., 2006; Zhou et al., 2008). Recently, some very good estimations were made regarding the AcAc+•OH reaction system at the M06-2X//M06-2X level (Ji et al., 2018). In order to systematically assess the atmospheric (day-time and night-time) chemistry of AcAc, the data obtained at the same level were adopted in this study although they were somewhat larger than the available experimental results. The Arrhenius expressions were also obtained and were given by: $k_{AcAc+O3}$ = 2.3 × 10^{-16} exp.(−685/T) and $k_{AcAc+NO3}$ = 4.21 × 10^{-16} exp.(−926/T) cm^3 molecule^{-1} s^{-1} for the AcAc+O$_3$ and AcAc+NO$_3$ reactions over the temperature range of 216–298 K, respectively. The rate constant at any temperature can be derived from these Arrhenius formulas within the measured temperature range. From the Arrhenius expressions, the activation energies were calculated to be 1.36 and 1.84 kcal mol^{-1} for the AcAc+O$_3$ and AcAc+NO$_3$ reactions within the investigated temperature range, respectively. This indicates that the ozonolysis of AcAc easily occurred with both the active species although AcAc+O$_3$ was slightly easier than the AcAc+NO$_3$ reaction within the measured temperature range.

In order to better assess the characteristic of AcAc+O$_3$/NO$_3$ reactions, the natural bond orbital (NBO) charges of $enol$-AcAc, O$_3$ and
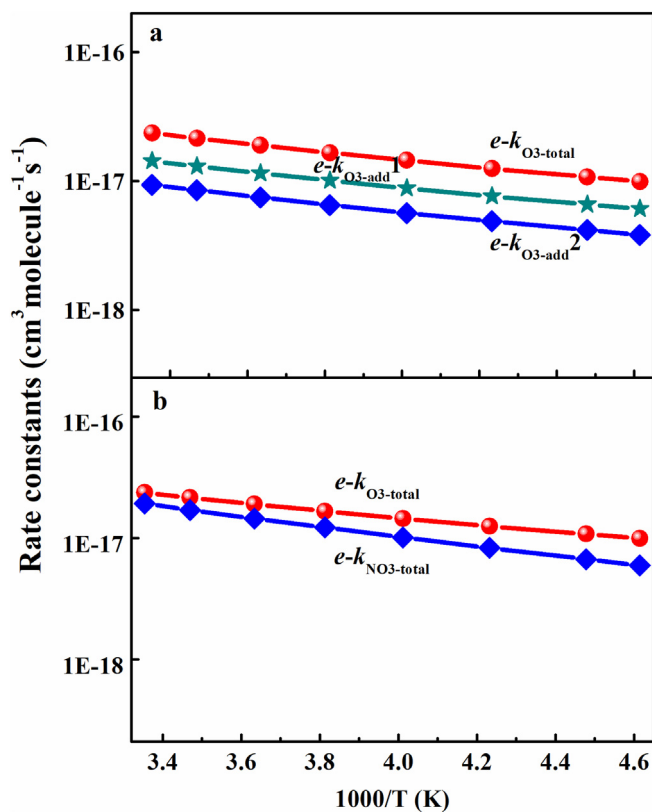

Fig. 2. (a) Rate constants of the major pathway in the AcAc+O$_3$ reaction and (b) the total rate constants of the AcAc+O$_3$ and AcAc+NO$_3$ reactions within the temperature range of 216–298 K (unit: cm^3 molecule^{-1} s^{-1}).

NO_3 are described and summarized in Fig. 3. The NBO charge of attracted-O atom in NO_3 was −0.332 e at the M06-2X/6-311G(d,p) level, which is two times negative than those of O atoms in O_3. Based upon this fact, the positive potential bond in *enol*-AcAc was more readily attacked by more negative nucleophiles (O_3 or NO_3). Furthermore, NO_3 addition to *enol*-AcAc was more favorable than O_3 addition from NBO results. On the contrary, from kinetic aspect (presented in Table S3), the rate constant of *e*-$R_{O3-total}$ pathway was larger than that of *e*-$R_{NO3-total}$ pathway. Combined with the mechanism results, it is mainly attributable to the existence of deep well along the reaction in the AcAc+NO_3 reaction system (Fig. 1) and the large exothermic energy in the AcAc+O_3 reaction system. In short, from both the mechanistic and kinetic aspects, the ozonolysis of AcAc is more important than that of NO_3 during the night-time hours.

3.2. Half-life of AcAc+O_3/NO_3 reaction

In order to further assess the atmospheric significance of the night-time chemistry of AcAc, it is necessary to estimate the half-life of AcAc +O_3/NO_3 reactions. First, the half-life of AcAc+O_3/NO_3 reaction was evaluated at the global level (Fig. S4 and Table S5). During the process, the concentrations of O_3 and NO_3 used were 7×10^{11} and 1×10^{10} molecules cm^{-3} in the troposphere, respectively (Logan, 1985; Atkinson, 1991). As shown in Fig. S4 and Table S5, the longer half-life revealed that the AcAc+NO_3 reaction was of minor importance relative to the AcAc+O_3 reaction. For example, the half-life of AcAc+NO_3 reaction was at least 1146.76 h at 298 K, which is about 86 times larger than that of AcAc+O_3 reaction (16.80 h). Then, considering a high concentration of O_3 in China, the half-life of AcAc+O_3 reaction ($\tau_{AcAc+O3}$) was assessed using [O_3] in the Pearl River Delta (PRD) and Yangtze River Delta (YRD) of China, which are the representative polluted areas in China. According to the results displayed in Fig. 4 and Table S6, under optimal conditions at the ground level in PRD ([O_3] = 5.50×10^{12} molecule cm^{-3}) (Liu et al., 2018) and YRD ([O_3] = 4.18×10^{12} molecule cm^{-3}) (Wang et al., 2017), the $\tau_{AcAc+O3}$ shortened and had values of 2.14 and 2.81 h at these two areas, respectively, which are much shorter than those at the global level. Additionally, the half-life of AcAc+O_3 reaction was estimated for Beijing (China), which has a larger [O_3] of 1.06×10^{13} molecule cm^{-3} (Table S6) (Wang et al., 2017). The

corresponding half-life value of the AcAc shortened and had the value of only 1.11 h. Since [O_3] was reduced at night-time through the deposition or reaction with NO (Zhang et al., 2004a), the predicted half-lives might have been under-estimated in this study. However, considering the fact that [O_3] in China is much higher than the global average concentration, the half-life of AcAc+O_3 reaction is not negligible. All the evidence highlights the atmospheric importance of AcAc+O_3 reaction in China during night-time hours. Therefore, in the proceeding experiments, the dominant product from ozonolysis of AcAc was calculated to evaluate the impact of night-time chemistry of AcAc in the atmosphere.

3.3. Subsequent reactions of primary ozonide and implications in the formation of SOA

As discussed earlier, POZ11 is obtained as the major product in the AcAc+O_3 reaction. Therefore, the concerted mechanism for the cleavage of primary ozonide (POZ11) was further considered. Concerted decomposition of POZ11 occurred with the cleavage of both the O—O and C—O bonds and formed a stable aldehyde or ketone along with a Criegee intermediate (carbonyl oxide; see Fig. 5a). The vibrational frequencies, absolute energies, Cartesian coordinates, and ZPEs of the relevant species are included in Table S7. Considering the PES shown in Fig. 5b, the decomposition of POZ11 through $TS_{POZ}1$ or $TS_{POZ}2$ yielded MG ($R_{POZ}1$) or AA ($R_{POZ}2$) with the ΔE values of 17.53 and 27.35 kcal mol^{-1}, respectively. The large ΔE difference (more than 9 kcal mol^{-1}) between the $R_{POZ}1$ and $R_{POZ}2$ indicates that the short chain Criegee intermediate (CI_{short}) prefers to be formed rather than the long chain one (CI_{long}). The rate constants were also calculated for the two pathways, with the values of 3.67 ($R_{POZ}1$) and 1.59×10^{-7} s^{-1} ($R_{POZ}2$) at 298 K, respectively. The $R_{POZ}2$ corresponded to the small rate constant. However, it could still produce AA and CI_{long}, which was due to the large exothermic energy for the formation of POZ11. The obtained results suggest that the most favorable products from the ozonolysis of AcAc are the MG, AA and CIs.

MG, AA, and CIs have been identified as the critical species, which lead to the formation of SOA (De Haan et al., 2006; Sipilä et al., 2010; Tan et al., 2010; Lim et al., 2013; De Haan et al., 2018; Hakala and Donahue, 2018). Furthermore, the organic acids, such as AA obtained in this work, have an important role in acid-base reactions (Qiu et al., 2011) and the formation and growth of new particles (Zhang et al., 2004b; Altieri et al., 2008). Specifically, the polymerization of small α-dicarbonyls (such as, MG and glyoxal) also represents a major source of SOA on urban, regional, and global scales (Tan et al., 2009; Zarzana et al., 2012; Marrero-Ortiz et al., 2019). Therefore, to assess the role of night-time chemistry of AcAc in the formation of SOA, the SOA production from MG (as an example) was subsequently estimated. First, to obtain the concentration of AcAc, a time series of AcAc measurements in Nanjing (China) were conducted using water clusters as the reagent ions. Here, AcAc is identified by its molecular peak ($m/z = 101.060$)
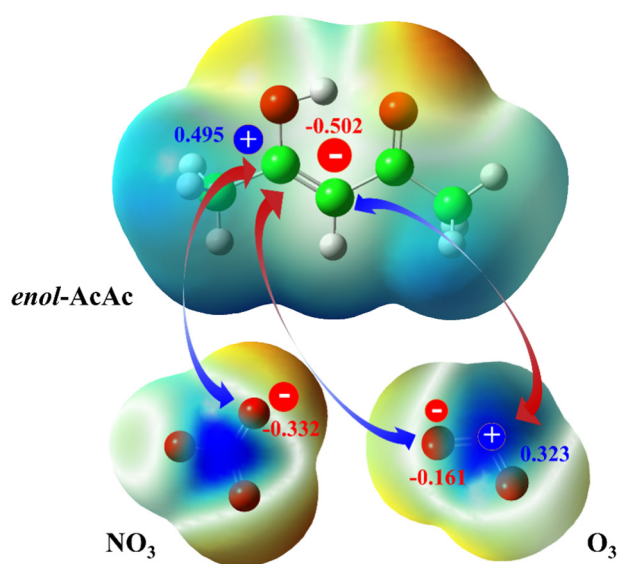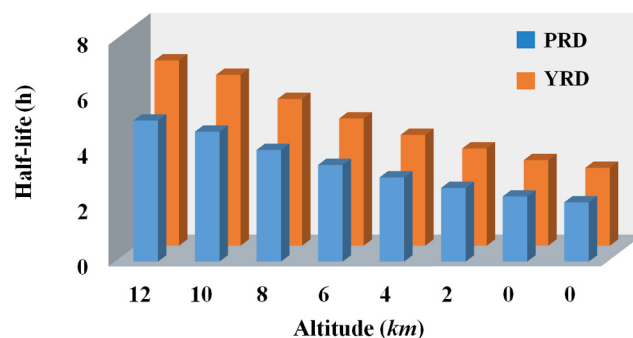

Fig. 3. The natural bond orbitals of *enol*-AcAc, O_3 and NO_3, with the blue and red colors depicting the maximum positive and negative charge densities, respectively (unit: e). (For interpretation of the references to colour in this figure legend, the reader is referred to the web version of this article.)

Fig. 4. Half-lives of the AcAc+O_3 reaction in PRD and YRD of China at the different altitudes (unit: h).
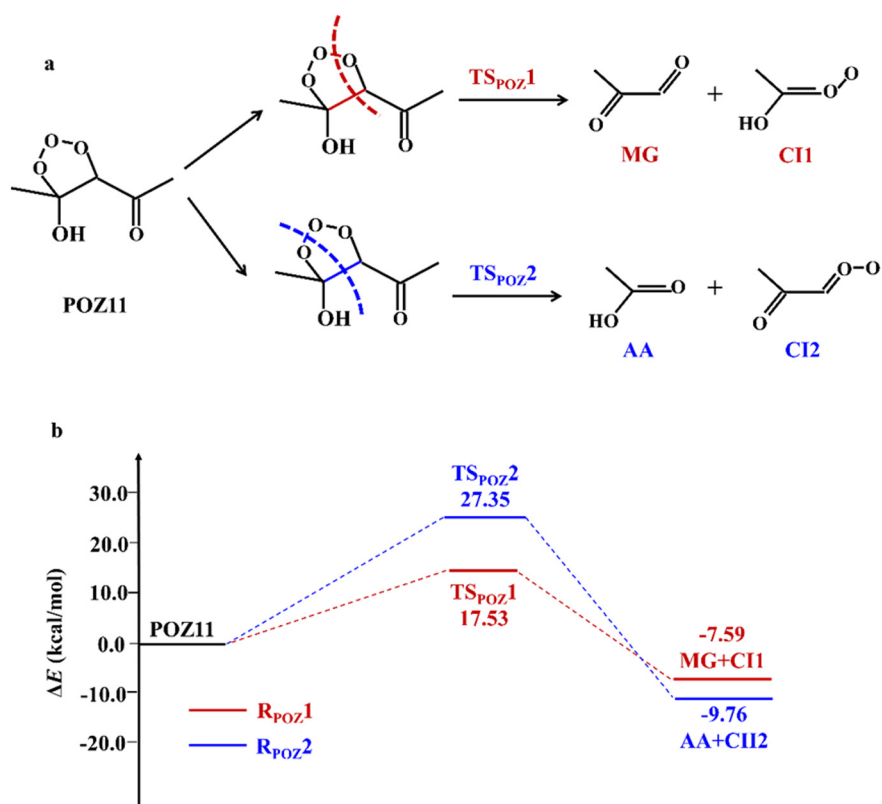
Fig. 5. (a) Scheme of the subsequent reactions of POZ11. (b) PES of the subsequent reactions of POZ11.

and its fragmentations at $C_3H_7O^+$ ($m/z = 59.049$) and $C_2H_3O^+$ ($m/z = 43.018$), which have been confirmed by spiking a high-resolution time-of-flight chemical ionization mass spectrometer (HR-ToF-CIMS) with pure AcAc sample. Additionally, the measured concentration of

AcAc shown in Fig. 6a indicates a diurnal variation in that location, which is possibly affected by the photochemical activity and the local emissions. As a result, the concentration of AcAc varied from 0.05 to 0.135 ppbv in Nanjing, China. Second, the production of SOA from MG
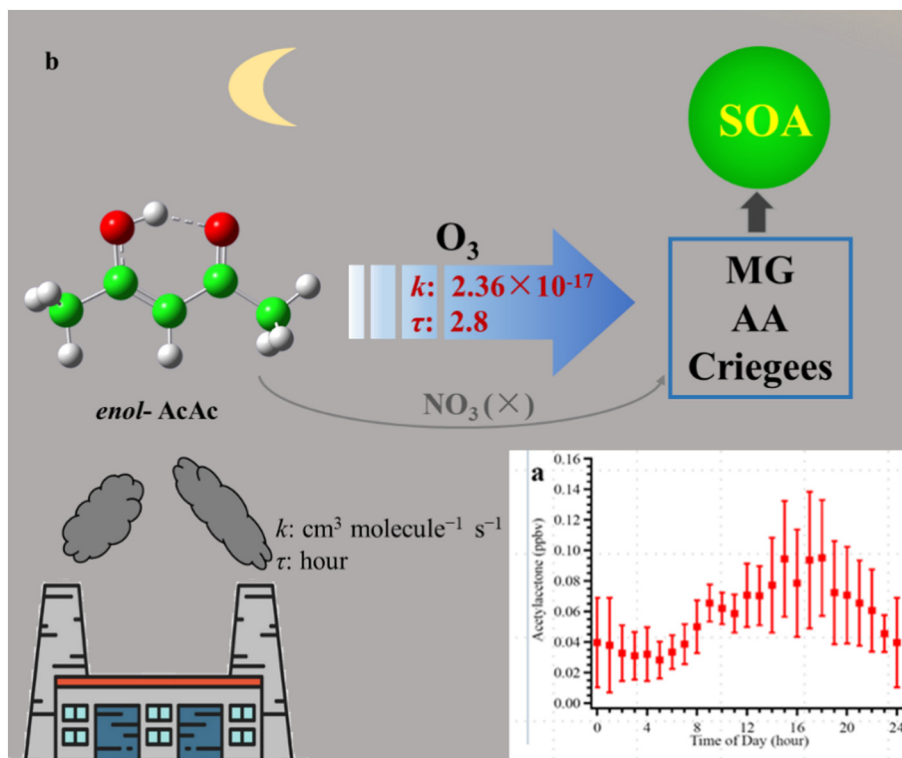

Fig. 6. (a) The diurnal profile of AcAc measured using the HR-ToF-CIMS method in Nanjing, China. (b) The role of the atmospheric chemistry of AcAc on the SOA and O_3 formation.

was estimated on the basis of the calculations and measurements, and the maximum value of SOA_{par} was found to be 3.31×10^9 molecules cm^{-3}. However, as for the values of SOA_{par} from another two major products of AA and CIs, the data cannot be deduced because of the absence of Y_i values. Therefore, the SOA_{par} value from MG and the night-time reactions of AcAc with O_3 can dominate the contribution to the formation of SOA.

4. Conclusions

The night-time chemistry of AcAc and its role in the formation of SOA were evaluated using theoretical calculations. The mechanism, kinetics, and the atmospheric fate of O_3- and NO_3-initiated oxidations of AcAc and the contribution to SOA yield were also explored. The ozonolysis of AcAc was found to be more favorable than the NO_3-initiated oxidation of AcAc because of longer half-life and smaller rate constant of AcAc $+NO_3$ reaction, suggesting that the NO_3-initiated oxidation of AcAc is less significant for the night-time chemistry of AcAc. The rate constant for the ozonolysis of AcAc was estimated to be 2.36×10^{-17} cm^3 molecule^{-1} s^{-1} at 298 K, whereas the half-life was about a few hours in several representative polluted areas in China. The longest half-life of ozonolysis of AcAc was obtained to be 2.8 h in the YRD of China under optimal conditions. Subsequently, the dominant product POZ11 from the ozonolysis reaction proceeded the cleavage of both the O—O and C—O bonds and formed MG or AA along with a Criegee intermediate. The corresponding rate constants were found to be 3.67 or 1.59×10^{-7} s^{-1}. Furthermore, the calculated SOA yield from MG was found to be 3.31×10^9 molecules cm^{-3}, suggesting that the night-time atmospheric reactions of AcAc can contribute to the formation of SOA.

In addition, the rate constants and half-lives of AcAc$+O_3$, as obtained in this work, and those of AcAc$+\bullet OH$ (Ji et al., 2018) reaction systems were compared. The atmospheric reaction of AcAc with $\bullet OH$ was found to be more significant than the AcAc with O_3 during day-time. However, due to the drop in concentration of $\bullet OH$ and increase in the concentration of O_3 during the night-time hours, the half-life of AcAc became more strongly related to the concentrations of higher O_3 during the night-time hours. Therefore, the ozonolysis of AcAc is of major significance in the night-time atmosphere and the formation of SOA. Considering the atmospheric reactivity of AcAc towards $\bullet OH$ and O_3, AcAc can successively contribute towards the formation of SOA during both the day-time and night-time hours due to very short reaction half-lives and non-negligible concentrations under polluted environments (Fig. 6b). The obtained results reveal that, with the development of industrialization and the increase of O_3 pollution, the importance of AcAc deserves more attention, especially to assess the impacts of AcAc on the formation of SOA using chemical transport models.

CRediT authorship contribution statement

Yuemeng Ji: Conceptualization, Software, Resources, Funding acquisition, Formal analysis, Writing - original draft, Writing - review & editing.**Dandan Qin:**Data curation, Validation, Writing - original draft, Formal analysis.**Jun Zheng:**Formal analysis, Data curation.**Qiuju Shi:** Writing - original draft.**Jiaxin Wang:**Visualization.**Qinhao Lin:**Visualization.**Jiangyao Chen:**Resources.**Yanpeng Gao:**Software, Visualization. **Guiying Li:**Writing - review & editing.**Taicheng An:**Supervision, Project administration, Writing - review & editing.

Declaration of competing interest

The authors declare that they have no known competing financial interests or personal relationships that could have appeared to influence the work reported in this paper.

Appendix A. Supplementary data

The structures, Cartesian coordinates, frequencies, zero-point energies, and absolute energies of all relevant species involved in the title reaction, along with the branching ratios, the rate constants, and the half-lives are listed in the Supporting Information. This material is available free of charge via the Internet. Supplementary data to this article can be found online at https://doi.org/10.1016/j.scitotenv.2020.137610.

References

Altieri, K.E., Seitzinger, S.P., Carlton, A.G., Turpin, B.J., Klein, G.C., Marshall, A.G., 2008. Oligomers formed through in-cloud methylglyoxal reactions: chemical composition, properties, and mechanisms investigated by ultra-high resolution FT-ICR mass spectrometry. Atmos. Environ. 42, 1476–1490.

Antonov, I., Voronova, K., Chen, M.W., Sztaray, B., Hemberger, P., Bodi, A., Osborn, D.L., Sheps, L., 2019. To boldly look where no one has looked before: identifying the primary photoproducts of acetylacetone. J. Phys. Chem. A 123, 5472–5490.

Aschmann, S.M., Arey, J., Atkinson, R., 1996. OH radical formation from the gas-phase reactions of O_3 with methacrolein and methyl vinyl ketone. Atmos. Environ. 30, 2939–2943.

Atkinson, R., 1991. Kinetics and mechanisms of the gas-phase reactions of the NO_3 radical with organic compounds. J. Phys. Chem. Ref. Data 20, 459–507.

Broadbent, S.A., Burns, L.A., Chatterjee, C., Vaccaro, P.H., 2007. Investigation of electronic structure and proton transfer in ground state acetylacetone. Chem. Phys. Lett. 434, 31–37.

Chuang, Y., Corchado, J.C., Truhlar, D.G., 1999. Mapped interpolation scheme for single-point energy corrections in reaction rate calculations and a critical evaluation of dual-level reaction path dynamics methods. J. Phys. Chem. A 103, 1140–1149.

De Haan, D.O., Tapavicza, E., Riva, M., Cui, T., Surratt, J.D., Smith, A.C., Jordan, M.C., Nilakantan, S., Almodovar, M., Stewart, T.N., Loera, A., De Haan, A.C., Cazaunau, M., Gratien, A., Pangui, E., Doussin, J.F., 2018. Nitrogen-containing, light-absorbing oligomers produced in aerosol particles exposed to methylglyoxal, photolysis, and cloud cycling. Environ. Sci. Technol 52, 4061–4071.

Ehn, M., Thornton, J.A., Kleist, E., Sipila, M., Junninen, H., Pullinen, I., Springer, M., Rubach, F., Tillmann, R., Lee, B., Lopez-Hilfiker, F., Andres, S., Acir, I.H., Rissanen, M., Jokinen, T., Schobesberger, S., Kangasluoma, J., Kontkanen, J., Nieminen, T., Kurten, T., Nielsen, L.B., Jorgensen, S., Kjaergaard, H.G., Canagaratna, M., Maso, M.D., Berndt, T., Petaja, T., Wahner, A., Kerminen, V.M., Kulmala, M., Worsnop, D.R., Wildt, J., Mentel, T.F., 2014. A large source of low-volatility secondary organic aerosol. Nature 506, 476–479.

Fernandez-Ramos, A., Ellingson, B.A., Garrett, B.C., Truhlar, D.G., 2007. Variational transition state theory with multidimensional tunneling. Rev. Comp. Ch. 23.

Finlayson-Pitts, B.J., Pitts, J.N., 1997. Tropospheric air pollution: ozone, airborne toxics, polycyclic aromatic hydrocarbons, and particles. Science 276, 1045–1051.

Frisch, M., Trucks, G., Schlegel, H.B., Scuseria, G., Robb, M., Cheeseman, J., Scalmani, G., Barone, V., Mennucci, B., Petersson, G., 2009. Gaussian 09, revision D. 01. Gaussian Inc, Wallingford CT.

Gao, Y., Wang, H., Zhang, X., Jing, S., Peng, Y., Qiao, L., Zhou, M., Huang, D., Wang, Q., Li, X., Li, L., Feng, J., Ma, Y., Li, Y., 2019. Estimating secondary organic aerosol production from toluene photochemistry in a megacity of China. Environ. Sci. Technol. 53, 8664–8671.

Haan, D., Loeffler, D.O., Koehler, K.W., C.A. N.M., P., 2006. Oligomer formation in evaporating aqueous glyoxal and methyl glyoxal solutions. Environ. Sci. Technol 40, 6318–6323.

Hakala, J.P., Donahue, N.M., 2018. Pressure stabilization of criegee intermediates formed from symmetric trans-alkene ozonolysis. J. Phys. Chem. A 122, 9426–9434.

Ho, Y., W, C., Chen, Y., Liu, C., 2015. Effects of molar ratio of Acetylacetone to aluminum precursor on the yttrium aluminum garnet ($Y_3Al_5O_{12}$, YAG) formation by a sol-gel process. InT.J. Appl. Ceram. Technol. 12, E53–E58.

Hoigne, J., Bader, H., 1978. Ozonation of water: kinetics of oxidation of ammonia by ozone and hydroxyl radicals. Environ. Sci. Technol. 12, 79–84.

Hollmann, F., Gumulya, Y., Tölle, C., Liese, A., Thum, O., 2008. Evaluation of the laccase from myceliophthora thermophila as industrial biocatalyst for polymerization reactions. Macromolecules 41, 8520–8524.

Holloway, A.-L., Treacy, J., Sidebottom, H., Mellouki, A., Daele, V., Le.Bras, G., Barnes, I.A., 2006. Kinetic and mechanistic study of atmospheric oxidation of 1,3-diketone. Proceedings of 19th International Symposium on Gas Kinetics. Orleans, France, pp. 61–62 , July 22-27.

Ishiwata, T., Tanaka, I., Kawaguchi, K., Hirota, E., 1985. Infrared diode laser spectroscopy of the NO_3 $\nu 3$ band. J. Chem. Phys. 82, 2196–2205.

Ji, Y., Gao, Y., Li, G., An, T., 2012. Theoretical study of the reaction mechanism and kinetics of low-molecular-weight atmospheric aldehydes (C1–C4) with NO_2. Atmos. Environ. 54, 288–295.

Ji, Y., Wang, H., Gao, Y., Li, G., An, T., 2013. A theoretical model on the formation mechanism and kinetics of highly toxic air pollutants from halogenated formaldehydes reacted with halogen atoms. Atmos. Chem. Phys. 13, 11277–11286.

Ji, Y., Zhao, J., Terazono, H., Misawa, K., Levitt, N.P., Li, Y., Lin, Y., Peng, J., Wang, Y., Duan, L., Pan, B., Zhang, F., Feng, X., An, T., Marrero-Ortiz, W., Secrest, J., Zhang, A.L., Shibuya, K., Molina, M.J., Zhang, R., 2017. Reassessing the atmospheric oxidation mechanism of toluene. Proc. Natl. Acad. Sci. U. S. A. 114, 8169–8174.

Ji, Y., Zheng, J., Qin, D., Li, Y., Gao, Y., Yao, M., Chen, X., Li, G., An, T., Zhang, R., 2018. OH-initiated oxidation of acetylacetone: implications for ozone and secondary organic aerosol formation. Environ. Sci. Technol. 52, 11169–11177.

Lim, Y.B., Turpin, B.J., Tan, Y., 2013. Chemical insights, explicit chemistry, and yields of secondary organic aerosol from OH radical oxidation of methylglyoxal and glyoxal in the aqueous phase. Atmos. Chem. Phys. 13, 8651–8667.

Liu, H., Liu, S., Xue, B., Lv, Z., Meng, Z., Yang, X., Xue, T., Yu, Q., He, K., 2018. Ground-level ozone pollution and its health impacts in China. Atmos. Environ. 173, 223–230.

Logan, J.A., 1985. Tropospheric ozone' seasonal behavior, trends, and anthropogenic influence. J. Geophys. Res. 90 (D6), 10463–10482.

Marrero-Ortiz, W., Hu, M., Du, Z., Ji, Y., Wang, Y., Guo, S., Lin, Y., Gomez-Hermandez, M., Peng, J., Li, Y., Secrest, J., Zamora, M.L., Wang, Y., An, T., Zhang, R., 2019. Formation and optical properties of brown carbon from small *a*-dicarbonyls and amines. Environ. Sci. Technol. 53, 117–126.

Mellouki, A., Bras, G.L., Sidebottom, H., 2003. Kinetics and mechanisms of the oxidation of oxygenated organic compounds in the gas phase. Chem. Rev. 103, 5077–5096.

Mellouki, A., Wallington, T.J., Chen, J., 2015. Atmospheric chemistry of oxygenated volatile organic compounds: impacts on air quality and climate. Chem. Rev. 115, 3984–4014.

Nagashima, N., Kudoh, S., Takayanagi, M., Nakata, M., 2001. UV-induced photoisomerization of acetylacetone and identification of less-stable isomers by low-temperature matrix-isolation infrared spectroscopy and density functional theory calculation. J. Phys. CheM.A. 105, 10832–10838.

Qiu, C., Wang, L., Lal, V., Khalizov, A.F., Zhang, R., 2011. Heterogeneous reactions of alkylamines with ammonium sulfate and ammonium bisulfate. Environ. Sci. Technol. 45, 4748–4755.

Raykar, V.S., Singh, A.K., 2010. Thermal and rheological behavior of acetylacetone stabilized ZnO nanofluids. Thermochimi. Acta. 502, 60–65.

Rissanen, M.P., Kurten, T., Sipila, M., Thornton, J.A., Kangasluoma, J., Sarnela, N., Junninen, H., Jorgensen, S., Schallhart, S., Kajos, M.K., Taipale, R., Springer, M., Mentel, T.F., Ruuskanen, T., Petaja, T., Worsnop, D.R., Kjaergaard, H.G., Ehn, M., 2014. The formation of highly oxidized multifunctional products in the ozonolysis of cyclohexene. J. Am. Chem. Soc. 136, 15596–15606.

Sareen, N., Waxman, E.M., Turpin, B.J., Volkamer, R., Carlton, A.G., 2017. Potential of aerosol liquid water to facilitate organic aerosol formation: assessing knowledge gaps about precursors and partitioning. Environ. Sci. Technol. 51, 3327–3335.

Shrivastava, M., Cappa, C.D., Fan, J., Goldstein, A.H., Guenther, A.B., Jimenez, J.L., Kuang, C., Laskin, A., Martin, S.T., Ng, N.L., Petaja, T., Pierce, J.R., Rasch, P.J., Roldin, P., Seinfeld, J.H., Shilling, J., Smith, J.N., Thornton, J.A., Volkamer, R., Wang, J., Worsnop, D.R., Zaveri, R.A., Zelenyuk, A., Zhang, Q., 2017. Recent advances in understanding

secondary organic aerosol: Implications for global climate forcing. Rev. Geophys. 55, 509–559.

Sipilä, M., Berndt, T., Petäjä, T., Brus, D., Vanhanen, J., Stratmann, F., Patokoski, J., Mauldin III, R.L., Hyvärinen, A.-P., Lihavainen, H., Kulmala, M., 2010. The role of sulfuric acid in atmospheric nucleation. Science 327, 1243–1246.

Tan, Y., Perri, M.J., Seitzinger, S.P., Turpin, B.J., 2009. Effects of precursor concentration and acidic sulfate in aqueous glyoxal-OH radical oxidation and implications for secondary organic aerosol. Environ. Sci. Technol. 43, 8105–8112.

Tan, Y., Carlton, A.G., Seitzinger, S.P., Turpin, B.J., 2010. SOA from methylglyoxal in clouds and wet aerosols: Measurement and prediction of key products. Atmos. Environ. 44, 5218–5226.

Tan, Y., Lim, Y.B., Altieri, K.E., Seitzinger, S.P., Turpin, B.J., 2012. Mechanisms leading to oligomers and SOA through aqueous photooxidation: insights from OH radical oxidation of acetic acid and methylglyoxal. Atmos. Chem. Phys. 12, 801–813.

Trivella, A., Roubin, P., Theule´, P., Coussan, S., Manca, C., 2007. UV and IR photoisomerization of acetylacetone trapped in a nitrogen matrix. J. Phys. CheM.A. 111, 3074-3081.

Tsujimoto, T., Uyama, H., Kobayashi, S., 2001. Polymerization of Vinyl monomers using oxidase catalysts. Macromol. Biosci. 1, 228–232.

Wang, H., Ji, Y., Gao, Y., Li, G., An, T., 2015. Theoretical model on the formation possibility of secondary organic aerosol from OH initialed oxidation reaction of styrene in the presence of O_2/NO. Atmos. Environ. 101 (1-9).

Wang, T., Xue, L., Brimblecombe, P., Lam, Y., Li, L., Zhang, L., 2017. Ozone pollution in China: A review of concentrations, meteorological influences, chemical precursors, and effects. Sci. Total. Environ. 575, 1582–1596.

Warneke, J., Willem, F, Van, D., Rudolf, P., Michal, S., Papp, P., Matejcik, S., Borrmann, T., Swiderek, P., 2015. Acetone and the precursor ligand acetylacetone: distinctly different electron beam induced decomposition? Phys. Chem. Chem. Phys. 17, 1204–1216.

Yuan, B., Hu, W., Shao, M., Wang, M., Chen, W., Lu, S., Zeng, L., Hu, M., 2013. VOC emissions, evolutions and contributions to SOA formation at a receptor site in eastern China. Atmos. Chem. Phys. 13, 8815–8832.

Zarzana, K.J., Haan, D. O. De., Freedman, M.A., Hasenkopf, C.A., Tolbert, M. A, 2012. Optical properties of the products of *a*-dicarbonyl and amine reactions in simulated cloud droplets. Environ. Sci. Technol 46, 4845–4851.

Zhang, R., Lei, W, Tie, X., Hess, P., 2004a. Industrial emissions cause extreme urban ozone diurnal variability. Proc. Natl. Acad. Sci. U. S. A. 101, 6346–6350.

Zhang, R., Suh, I., Zhao, J., Zhang, D., Fortner, E.C., Tie, X., Molina, L.T., Molina, M.J., 2004b. Atmospheric new particle formation enhanced by organic acids. Science 304, 1487–1490.

Zhang, R., Wang, G., Guo, S., Zamora, M., Ying, Q., Lin, Y., Wang, W., Hu, M., Wang, Y., 2015. Formation of urban fine particulate matter. Chem. Rev. 115, 3803–3855.

Zhang, Y., Wang, X., Wen, S., Herrmann, H., Yang, W., Huang, X., Zhang, Z., Huang, Z., He, Q., George, C., 2016. On-road vehicle emissions of glyoxal and methylglyoxal from tunnel tests in urban Guangzhou, China. Atmos. Environ. 127, 55–60.

Zheng, J., Zhang, S., Lynch, B., Corchado, J., Chuang, Y., Fast, P., Hu, W., Liu, Y., Lynch, G., Nguyen, K., 2010. POLYRATE, version 2010-A; Software Manager. University of Minnesota, Minneapolis, MN.

Zhou, S., Barnes, I., Zhu, T., Bejan, I., Albu, M., Benter, T., 2008. Atmospheric chemistry of acetylacetone. Environ. Sci. Technol. 42, 7905–7910.